SUPPLEMENTAL MATERIAL

Role of ultrastructural determinants of glomerular permeability in ultrafiltration function loss

Andrea Remuzzi [1], Sara Conti [2], Bogdan Ene-Iordache [2], Susanna Tomasoni [2],

Paola Rizzo [2], Ariela Benigni [2] and Giuseppe Remuzzi [2,3]

[1] *University of Bergamo, Via Marconi 5, 24144, Dalmine, Italy*

[2] *Istituto di Ricerche Farmacologiche Mario Negri IRCCS, Via Stezzano, 87 - 24126 Bergamo*

[3] *L. Sacco Department of Biomedical and Clinical Sciences, University of Milan, 20122 Milan, Italy*

A.R. and S.C. contributed equally to this study.

Table of Contents

Theoretical modeling of the hydraulic resistance of glomerular capillary wall

The structure of the glomerular capillary wall, as well as of its components, are highly complex. Here we considered the glomerular filtration barrier (GFB), i.e. the filtering portion of the capillary wall composed of the three parallel layers: *i)* fenestrated endothelial layer (ENL); *ii)* glomerular basement membrane (GBM); *iii)* epithelial layer (EPL) composed of podocyte foot processes and filtration slits. We also considered the subpodocyte space (SPS), formed under the podocyte cell body and the anchoring processes attached to the GBM (1), that creates additional resistance to water flow after passing the GFB, and before entering the Bowman's space. While it has been neglected in older models of glomerular capillary wall permeability based on ultrastructure (2–4), a more recent study by Neal et. al (5) revealed that SPS in reality produces an important restriction to ultrafiltrate flow. This increased hydraulic resistance is attributable mainly to water movement along the SPS and to the constriction of fluid flow in narrow exit channels, termed *SPS exit pores* (SEP). Subsequently the same research group (6) developed a theoretical model of glomerular filtration based on ultrastructural data of SPS and SEPs.

Overall approach of the mathematical model

Since there are portions of the filtering surface area (FSA) of the capillary wall either uncovered or covered by SPS, there are two parallel pathways for filtration (6). If we denote with subscript 1 the characteristics of uncovered part and with 2 those of the covered portion, the total resistance (R_{TOT}) of the two parts in parallel is given by:

$$\frac{1}{R_{TOT}} = \frac{1}{R_1} + \frac{1}{R_2} \qquad\qquad (1)$$

The uncovered part of the FSA is composed of bare GFB and its resistance is the sum of resistances in series of each component layer:

$$R_1 = R_{GFB} = R_{ENL} + R_{GBM} + R_{EPL} \quad (1a)$$

The resistance of the FSA part covered by SPS is a sum of resistances in series, i.e. of the resistance of GFB that underlies the SPS, the resistance of SPS itself and of the adjacent SEPs:

$$R_2 = R_{GFB} + R_{SPS} + R_{SEP} \quad (1b)$$

In terms of hydraulic permeabilities and respective surface area, equation (1) can be written as:

$$k_{TOT} \cdot FSA = k_1 \cdot A_1 + k_2 \cdot A_2 \quad (2)$$

where A_1 and A_2 are the filtering surface area uncovered and covered by the SPS, respectively. According to the model of Neal et al. (6), the effect of partial SPS coverage on the overall hydraulic permeability can be estimated as a function of the fractional area ε of the FSA covered by SPS (A_2/FSA):

$$k_{TOT} = (1 - \varepsilon)k_1 + \varepsilon k_2 \quad (3)$$

We firstly calculated the total permeability (k_{TOT}) of glomerular capillary wall on the basis of functional data measured experimentally in micro-puncture studies (2,3) in the same strain of rats. Then, we used computational fluid dynamics (CFD) analysis of 3D models informed by ultrastructural data of ENL, GBM, and EPL to estimate the hydraulic permeability of bare GFB. To take into account the effect of partial SPS coverage we used the theoretical model by Neal et al. (6), as explained in the following. We then estimated the value of ε that allows to obtain total permeability equal to that derived from micro-puncture data. Due to uncertainty of SEP parameters, we also used a sensitivity analysis to estimate a range of ε values for the three experimental groups.

Total hydraulic permeability of glomerular capillary wall

To estimate the total hydraulic permeability of glomerular capillary wall we need to assume several functional parameters of the modeled kidney filtration barrier, in our case those of rat glomerulus. We used data from micro-puncture studies performed in the past by our group (4) in MWF and MWF-treated rats at 20 weeks of age, the age when micropuncture data have been usually performed. Body weight of these animals was in average 380 g. Whereas for Wistar rats we assumed data from the studies by Maddox et al. (3) and by Pinnick & Savin (7), performed in rats of approximately of 20 weeks of age, as reported in Supplemental Table 1.

Supplemental Table 1. Assumed micro-puncture functional data for glomerular ultrafiltration of rat.

	SNGFR	FSA	P_{GC}	P_{BS}	K_D (11)	K_f	k_{TOT}
	$(nL\ min^{-1})$	(mm^2)	$(mmHg)$	$(mmHg)$	(nm^2)	$(nL\ s^{-1}\ mmHg^{-1})$	$(m\ s^{-1}\ Pa^{-1})$
Wistar (3)	28.0	0.16 (7)	44	12	2.1	0.078	3.66E-09
MWF (4)	46.9	0.34	51	13	2.0	0.061	1.35E-09
MWF+lis (4)	54.6	0.31	44	13	2.2	0.126	3.05E-09

Legend: SNGFR, single nephron glomerular filtration rate; FSA, filtering surface area; P_{GC}, experimentally measured pressure in the glomerular capillary; P_{BS}, pressure measured in the Bowman's space; K_D, Darcy's permeability; K_f, ultrafiltration coefficient; k_{TOT}, total permeability of capillary wall. Numbers in parenthesis are referenced studies.

By definition, the total permeability of glomerular capillary wall is given by the ultrafiltration coefficient (K_f) divided by the glomerular FSA:

$$k_{TOT} = \frac{K_f}{FSA} \qquad\qquad (4)$$

The values of k_{TOT} (in S.I. units) for these three group-specific rats are shown in the last column of Supplemental Table 1.

Hydraulic permeability of the GFB

For the assessment of permeability of the GFB without SPS coverage, and the relative contribution of every single structural layer in eq. (1a), we followed the approach used by Drumond and Deen (8), using CFD to determine velocity and pressure fields during water filtration across the GFB. We considered a three-dimensional, parametric model of a unit cell based on a single filtration slit as shown in Figure 3. The model is composed of the three layers that jointly determine its functional properties: ENL, GBM and EPL and is periodic in the X- and Y-directions, while filtration occurs in the positive Z-direction.

Size of the unit cell of the GFB. We assumed the width (W) of the cell based on previous morphometrically measurements of glomerular capillary ultrastructure in these strains of rats (9). Thus, the width of the cell can be calculated as:

$$W = \frac{FSA}{TSL} \qquad (5)$$

where TSL is the total slit length of peripheral capillaries. Since TSL was not available for Wistar rats in previous studies, here we measured their filtration slit frequency (FSF). Then we calculated the width of the cell for the Wistar group with the formula (10):

$$W = \frac{2}{\pi} \cdot \frac{1}{FSF} \qquad (6)$$

where $\frac{2}{\pi}$ is a correction factor that accounts for the random angle of section. The length (L) of the cell was determined based on the epithelial slit pore frequency in such a way as to cover 50 pores, as measured in the present study for each group (Table 2). Since we need to simulate the passage of water through the membrane, the 3D fluid domain is the blue shape shown in Figure 3C. We

5

assumed the height of the fluid domain in order to achieve enough hydraulic length for the fluid to develop.

Endothelial layer. We designed the endothelial layer similarly in all rat groups, with a rhomboidal arrangement of fenestrae, as shown in Figure 3C, while the diameter ($D_{ENL\ f}$) follows normal distribution, as measured previously (11). Moreover, the ENL fenestrae were designed with different radii of curvature ($Rc_{ENL\ fi}$) toward the capillary lumen and ($Rc_{ENL\ fs}$) and toward the GBM (inset picture in Figure 3B).

GBM. The GBM was modeled as a homogeneous porous stratum between the ENL and EPL layers; its thickness was set equal to the average thickness in each rat group measured in this study (Table 2).

Epithelial layer. As shown before, epithelial layer length is different for each group, depending on the frequency of EPL slit pores. All EPL models were designed to have 50 slit pores, but each one has its own diameter ($D_{EP\ sp}$) distribution, as measured in the present study (Figure 3, A to C). We assumed the same radius of curvature ($R_{cEP\ sp}$) for epithelial slit pores for all groups (inset picture in Figure 3B). Finally, we assumed the dimensions of foot-processes (W_{FP}, $H_{FP,}$ see Figure 3B and Table 4) as measured previously by our group in the same rat groups (9).

All the above structural layers were designed in *FreeCad* (v. 0.17, https://www.freecadweb.org) using homemade scripts in *python* (v. 2.7, https://www.python.org) tailored to each rat group.

Computational fluid dynamics of water passage across the GFB

After creating the GFB model, the 3D space of the fluid passing through the GFB was exported in .STL file format. Numerical grids of hexahedral cells were created with the *snappyHexMesh* pre-processor of the *OpenFOAM* CFD tool-box (v 6, https://openfoam.org). Fine meshes composed of more than 3 million cells were generated for all three models; a section view of the MWF mesh is shown in Figure 3C (right). For the CFD simulation we assumed that water filtered would be at a temperature of 37° C, having constant density $\rho = 0.9933$ g cm^{-3} and constant (Newtonian) viscosity $\mu = 0.007$ g cm^{-1} s^{-1}. Both GBM and glycocalyx were treated as total porous mediums. Regarding the porous properties of the GBM, we assumed group-specific Darcy permeability (K_D, in nm^2), as measured experimentally by us in the same rat strains (12). Since it depended non-linearly on the transmembrane hydraulic pressure drop applied during experiments, we used non-linear fitting of K_D of GBM layers in the absence of albumin (12) to determine the group-specific permeability for Wistar, MWF and MWF-treated rats (Supplemental Table 1). We also assumed that endothelial fenestrae are filled with glycocalix (8) for which we used a value of Darcy's permeability of 2.7 nm^2 as previously reported (8). On the bottom side of the fluid domain, we imposed constant flow calculated as SNGFR by the fractional area of the model and FSA. On the walls, corresponding to ENL fenestrae, EPL pores and foot-processes, a no-slip condition was imposed. A boundary condition of symmetric flow was imposed on all other vertical surfaces, and a zero-pressure condition was assumed at the top wall representing the outlet of the fluid domain.

The numerical simulations were carried out using the *porousSimpleFoam* solver from the *OpenFOAM* suite, which is a steady state solver dedicated to porous mediums.

Results of the CFD simulations

Numerical simulations allowed to calculate velocity and pressure fields within the 3D domains of the GFB. An example of water velocity distribution for a representative unit cell of GFB is shown in the Supplemental Figure 1.
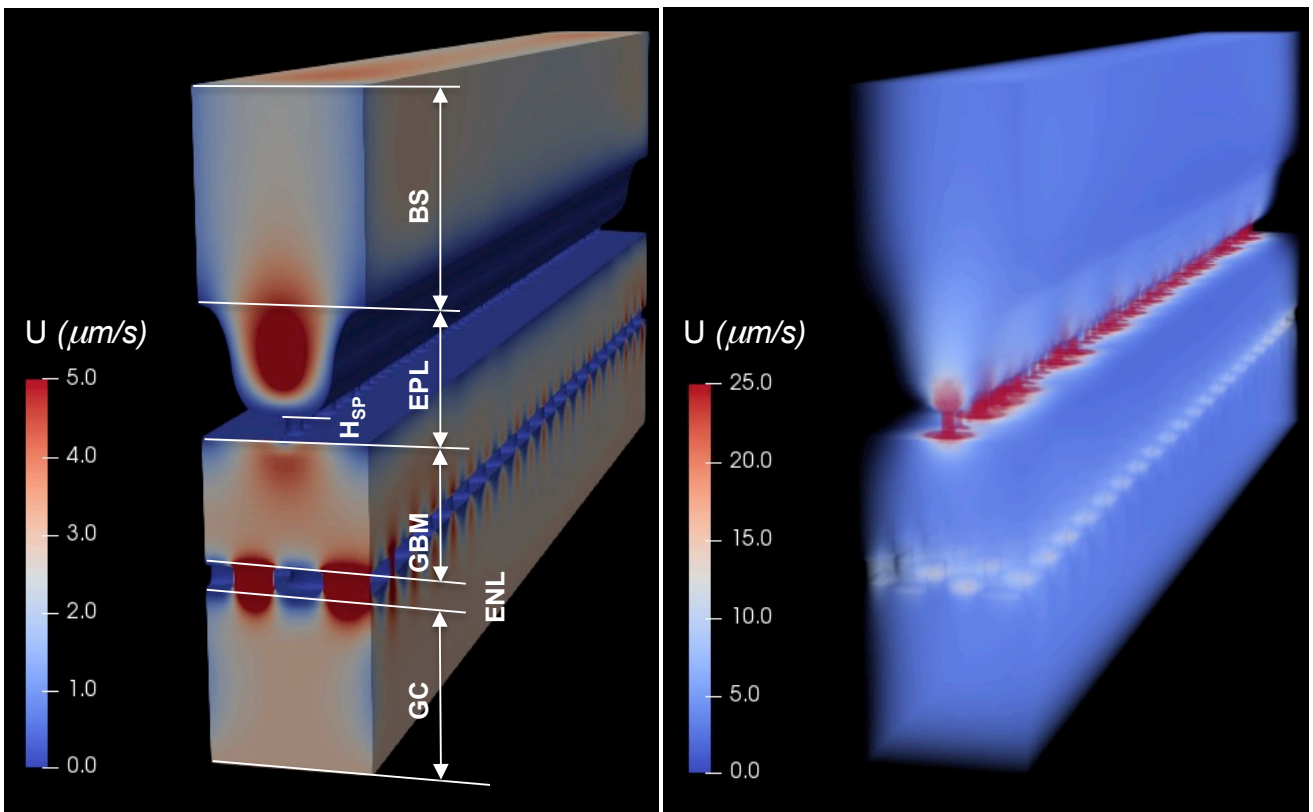
Supplemental Figure 1. Water velocity through a representative model of GFB (MWF+lis). Plot of velocity on the walls of the model (*left*). Volume rendering of velocity magnitude inside the GFB (*right*). GC, glomerular capillary; ENL; endothelial layer; GBM, glomerular basement membrane; H_{SP}, height of slit pores; EPL, epithelial layer; BS, Bowman's space.

Velocity distribution reveals that filtered water is, as expected, accelerated in the ENL fenestrae, but the highest velocities (red color) occur within the EPL slit pores due to the enormous narrowing of the cross-sectional area for water passage.

8

The pressure drop over the GFB models for Wistar, MWF and MWF-treated rats is shown in the Supplemental Figure 2.
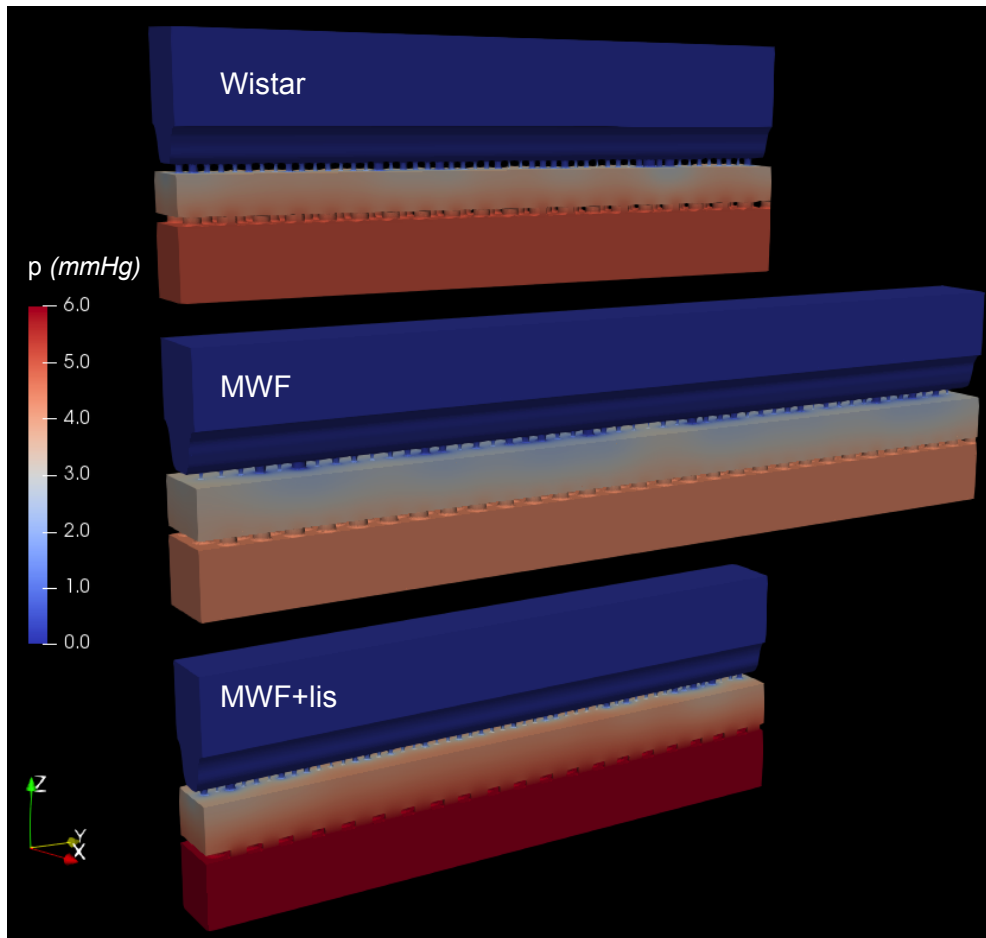
Supplemental Figure 2. Pressure drop over the GFB for Wistar, MWF and MWF+lis rats. The highest pressure drop occurs in MWF+lis, then in Wistar and MWF.

It can be observed that the endothelial layer does not create a high pressure drop while the GBM determines a greater pressure decrease due to its porous nature. The highest pressure gradients take place in the epithelial slit pores, where the velocity of filtered water is the highest in absolute.

Calculation of GFB total and relative permeability. Once the pressure drop is known, the hydraulic permeability of every structural layer of GFB may be calculated as:

$$k_i = \frac{J_V}{\Delta P_i} \qquad (7)$$

where J_v is the volume flux averaged over the cross-sectional area, and the subscript i refers to each layer (ENL, GBM, EPL) or the whole GFB. The results are presented in the Supplemental Table 2.

Supplemental Table 2. CFD-predicted hydraulic permeability of the GFB with the relative contribution of each structural layer.

	k_{GFB}	k_{ENL}	k_{ENL}/k_{GFB}	k_{GBM}	k_{GBM}/k_{GFB}	k_{EPL}	k_{EPL}/k_{GFB}
Wistar	4.30E-09	3.00E-08	14.3%	1.49E-08	28.8%	7.56E-09	56.8%
MWF	3.52E-09	2.32E-08	15.2%	1.04E-08	33.9%	6.93E-09	50.9%
MWF+lis	3.77E-09	2.41E-08	13.5%	1.13E-08	28.9%	5.67E-09	57.6%

Legend: k, hydraulic permeability in $m \cdot s^{-1} \cdot Pa^{-1}$ and relative contribution to the total resistance of GFB in %; k_{GFB}, CFD calculated permeability of glomerular filtration barrier; k_{ENL}, CFD calculated permeability of endothelial layer; k_{GBM}, CFD calculated permeability of glomerular basement membrane; k_{EPL}, CFD calculated permeability of epithelial layer.

The effect of partial SPS coverage on total permeability

As expected, the computed hydraulic permeability of the GFB (Supplemental Table 2) is higher than the total hydraulic permeability of the glomerular capillary wall (Supplemental Table 1), since the CFD model does not include the SPS domain, and the numerical results represent the hydraulic permeability (and resistance) of naked GFB. In order to estimate the contribution of SPS on the overall hydraulic resistance of the glomerular capillary wall, we used the theoretical model of Neal et al. (6). According to this model, the ratio between the total capillary wall permeability (k_{TOT}) consisting of GFB and partial SPS coverage, to that of the GFB (k_{GFB}) alone can be expressed as:

$$\frac{k_{TOT}}{k_{GFB}} = 1 - \frac{\varepsilon B}{1+B} \qquad (8)$$

where B is the ratio between the resistance of SPS including SEPs and that of underlying GFB. Based on this model (6), B can be calculated as:

$$B = \frac{R_{SPS}+R_{SEP}}{R_{GFB}} = \frac{GI_0(G)}{2I_1(G)} - 1 + \frac{128\mu\delta ka^2}{nb^4} \qquad (9)$$

where $G = \left(\frac{12\mu ka^2}{h^3}\right)^{0.5}$, with $I_0(G)$ and $I_1(G)$ being modified Bessel functions of first kind of order 0

and 1, respectively, μ is the dynamic viscosity of water, δ is the SEP length, k is the permeability of

GFB, a is the mean SPS radius, h is the SPS height, b is the SEP diameter and n is the number of SEP

channels for one SPS.

Ultrastructural parameters for the analytical modelling of SPS

We calculated or assumed group-specific parameters to be used as input data in equation (9), as

presented in Supplemental Table 3. We assumed the value of mean SPS radius (a) for Wistar rats in

line with the measurements of Neal et al (6). We then assumed the values of a for the two MWF

groups on the basis of the relative increase in SPS area for each podocyte, estimated by the SPS

volume for each podocyte and SPS mean height, as compared to normal Wistar rats. For this

calculation the mean number of podocytes per glomerular tuft for these three rat groups was

derived from values that we have previously reported (13). We also assumed values of SEP length,

SEP diameter and number of adjacent SEPs, as those reported by Neal et al (6) considering them

constant for the three rat groups. The viscosity of ultrafiltrate was assumed to be equal to 7.0 x 10^{-4}

Pa s (water at 37°C).

Supplemental Table 3. Ultrastructural parameters used for the analytical modelling of
SPS and SEP resistances.

Parameter	Unit	Wistar	MWF	MWF+lis	Notes
a	(μm)*	20.1	35.17	20.07	calculated
h	(μm)	0.34	0.69	0.54	measured
δ	(μm)	0.25 [0.1 - 0.5]	0.25 [0.1 - 0.5]	0.25 [0.1 - 0.5]	assumed (5),(6)
b	(μm)	0.15 [0.1 - 0.2]	0.15 [0.1 - 0.2]	0.15 [0.1 - 0.2]	assumed (6)
n		22	22	22	assumed (6)
k	($m\ s^{-1}Pa^{-1}$)	4.30E-09	3.52E-09	3.77E-09	CFD calculated

Legend: *a*, SPS mean radius; *h*, SPS mean height; *δ*, SEP length; *b*, SEP diameter; *n*, the number of SEPs for one SPS; *k*, permeability of GFB without SPS; *, all µm units should be transformed in m.

## Calculation of the fractional area covered by SPS

For a defined set of structural parameters (*a, h, δ, b, n*), it is possible to compute the value of B and then calculate the total capillary wall resistance (R_{TOT}) on the basis of GFB resistance of (R_{GFB}):

$$\frac{R_{GFB}}{R_{TOT}} = \frac{k_{TOT}}{k_{GFB}} = 1 - \frac{\varepsilon B}{1+B} \qquad (10)$$

Rearranging equation (10)

$$R_{TOT} = R_{GFB}\left(\frac{1+B}{1-\varepsilon B+B}\right) \qquad (11)$$

We then calculated the value of ε for which calculated R_{TOT} equals the value estimated by measured K_f (see Supplemental Table 1). The effect of SPS coverage on calculated total hydraulic resistance R_{TOT} as a function of ε for a representative group of rats is shown in the Supplemental Figure 3.
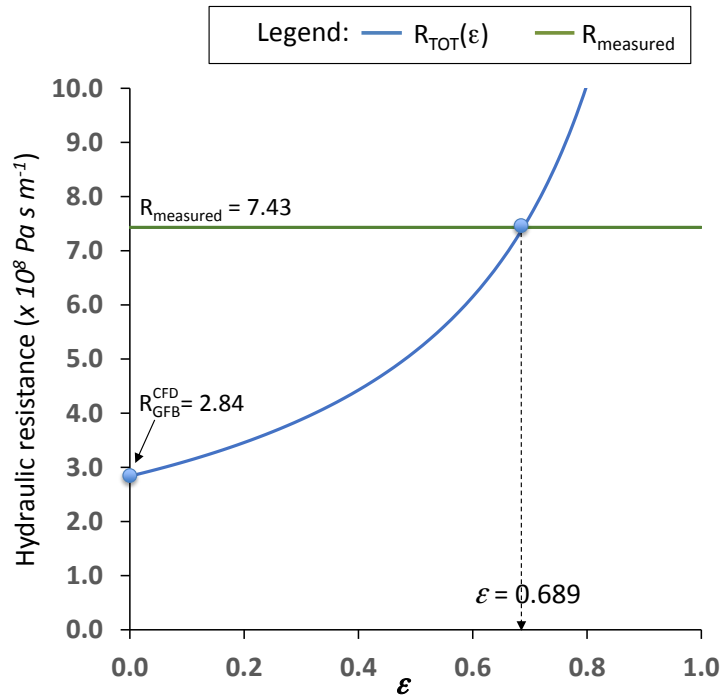
Supplemental Figure 3. The effect of SPS coverage on the hydraulic resistance for a representative group (MWF) of rats. These relationships were generated using as input data: a = 35.17 µm, h = 0.69 µm, d = 0.25

12

μm, b = 0.15 μm and n = 22. The value of ε was calculated as the value of R_{TOT} (eq. 11) equals that derived from measured K_f.

It should be noted that ε can take values between 0 and 1, with 0 meaning a glomerular capillary FSA without SPS coverage and 1 a FSA fully covered by SPS. For ε=0, the total hydraulic resistance is equal to that of GFB previously calculated by CFD. As ε is increasing, the total resistance R_{TOT}, consisting of both uncovered parts of FSA and parts covered by SPS, starts to increase non-linearly. We used this model to derive the values of ε for which R_{TOT} reaches the experimentally measured resistance of glomerular capillary wall for the three groups of rats, for a set of the assumed parameters δ (SEP length) and b (SEP diameter).

Estimation of pressure in SPS

According to the model of Neal et al (6), the mean pressure in the SPS can be calculated from the relation:

$$P_{SPS} = \frac{BP_{GC} + P_{BS}}{1+B} \qquad (12)$$

where P_{GC} is the pressure inside the glomerular capillary lumen and P_{BS} is the pressure in Bowman's capsule (Supplemental Table 1). We used equation (12) to estimate the pressures within the SPS of the three rat groups. The value of P_{BS} together with the value of the surface area of the SPS (given by the product of ε and FSA) and the mean number podocyte per glomerular tuft, allowed estimating a range of the hydrodynamic force acting on a single podocyte cell body (see main text). Calculated pressures in SPS and forces acting on a single podocyte cell body for the three rat groups are reported in Table 3, while the total hydraulic resistance of glomerular capillary wall considering the partial contribution of SPS coverage are presented in Figure 4 in the main manuscript.

13

References

1.   Neal CR. Podocytes … What's Under Yours? (Podocytes and Foot Processes and How They Change in Nephropathy). *Front. Endocrinol.* 2015;6:9.

2.   Deen WM, Troy JL, Robertson CR, Brenner BM. Dynamics of glomerular ultrafiltration in the rat. IV. Determination of the ultrafiltration coefficient. *J. Clin. Invest.* 1973;52(6):1500–1508.

3.   Maddox DA et al. Determinants of glomerular filtration in experimental glomerulonephritis in the rat. *J. Clin. Invest.* 1975;55(2):305–318.

4.   Remuzzi A, Puntorieri S, Battaglia C, Bertani T, Remuzzi G. Angiotensin converting enzyme inhibition ameliorates glomerular filtration of macromolecules and water and lessens glomerular injury in the rat. *J. Clin. Invest.* 1990;85(2):541–549.

5.   Neal CR, Crook H, Bell E, Harper SJ, Bates DO. Three-dimensional reconstruction of glomeruli by electron microscopy reveals a distinct restrictive urinary subpodocyte space. *J. Am. Soc. Nephrol. JASN* 2005;16(5):1223–1235.

6.   Neal CR et al. Glomerular filtration into the subpodocyte space is highly restricted under physiological perfusion conditions. *Am. J. Physiol. Renal Physiol.* 2007;293(6):F1787-1798.

7.   Pinnick RV, Savin VJ. Filtration by superficial and deep glomeruli of normovolemic and volume-depleted rats. *Am. J. Physiol.* 1986;250(1 Pt 2):F86-91.

8.   Drumond MC, Deen WM. Structural determinants of glomerular hydraulic permeability. *Am. J. Physiol.* 1994;266(1 Pt 2):F1-12.

9.   Iordache BE et al. Effects of angiotensin-converting enzyme inhibition on glomerular capillary wall ultrastructure in MWF/Ztm rats. *J. Am. Soc. Nephrol. JASN* 1994;5(6):1378–1384.

14

10. Drumond MC, Kristal B, Myers BD, Deen WM. Structural basis for reduced glomerular filtration capacity in nephrotic humans. *J. Clin. Invest.* 1994;94(3):1187–1195.

11. Tsuji K et al. Re-characterization of the Glomerulopathy in CD2AP Deficient Mice by High-Resolution Helium Ion Scanning Microscopy. *Sci. Rep.* 2017;7(1):8321.

12. Macconi D et al. Effect of angiotensin-converting enzyme inhibition on glomerular basement membrane permeability and distribution of zonula occludens-1 in MWF rats. *J. Am. Soc. Nephrol. JASN* 2000;11(3):477–489.

13. Macconi D et al. Podocyte repopulation contributes to regression of glomerular injury induced by ACE inhibition. *Am. J. Pathol.* 2009;174(3):797–807.